Journal of Imaging Science and Technology® 52(3): 030504–030504-8, 2008.

The Learning-Based Principal Component Analysis Technique in Low Resolution and High Resolution Spectral Images

Vladimir Bochko
Department of Information Technology, Lappeenranta University of Technology, P.O. Box 20, 53851 Lappeenranta, Finland
E-mail: botchko@cs.joensuu.fi

Yoichi Miyake▲
Department of Information and Image Sciences, Chiba University, 1-33 Yayoi-cho, Inage-ku, Chiba 263-8522, Japan

Jussi Parkkinen▲
Department of Computer Science, University of Joensuu, 80101 Joensuu, Finland

Abstract. *This paper presents a learning-based principal component analysis technique for accurate representation of spectral color in low and high resolution spectral images. Three learning techniques, LLE, ISOMAP, and regressive principal component analysis (PCA), are studied for this purpose. The basic concepts for the regressive PCA technique, which is computationally efficient and represents a combination of standard PCA and regression, are examined. To utilize dimensionality reduction techniques such as LLE and ISOMAP as parametric mapping procedures, the methods must be modified by combining them with a regression approach which provides data mapping from a low-dimensional space to the input space. The LLE, ISOMAP, and regressive PCA learning techniques are compared with standard PCA using low-resolution spectral images. We show that the LLE and ISOMAP approaches are computationally demanding and are not well suited to high resolution image analysis. Regressive and standard PCA are then used in a test with high resolution spectral images. The comparative study based on the S-CIELAB* ΔE *and RMSE employs regressive PCA measures to illustrate accurate color representation.* © *2008 Society for Imaging Science and Technology.*
[DOI: 10.2352/J.ImagingSci.Technol.(2008)52:3(030504)]

INTRODUCTION

Telemedicine, network museums, network shopping, electronic money, digital archives, mobile phones with a digital camera, digital TV, digital copies, digital cameras, and electronic paper require the development of a high-quality color imaging system.[1] The images acquired by color imaging systems based on three channels are, however, not very accurate. To provide high quality in these systems, spectral (multicomponent) imaging systems are introduced. However, the large number of components requires additional memory to store the data and increases computational time. A recent study shows that eight channels or more are usually required to get an accurate color reproduction of images; alternatively, using the principal components of the image also permit a more accurate representation of the spectra.[2] It is also very useful in spectral image processing (low- and high-pass filtering, wavelet transforms, etc.) to apply a preprocessing step by reducing the dimensionality of an image containing dozens or hundreds of components to several components. The PCA technique is usually utilized for this purpose and saves computational time and memory. To make this algorithm more efficient, a technique incorporating not only information from retained principal components but from higher-order (weak) principal components (PCs) as well without changing the number of principal components is required. A possible solution to the problem is to use a learning technique incorporating the nonlinearity of data.

The basic techniques for nonlinear PCA and nonlinear dimensionality reduction include generative topographic mapping (GTM), Bayesian nonlinear factor analysis (Bayesian NFA), locally-linear embedding (LLE), and ISOMAP.[3–6] In addition, regressive PCA, which is simple and computationally efficient, is considered.[7] Regressive PCA has been successfully used to estimate the spectral reflectance of paintings[8] and to colorize gray-level images.[9] A limitation of the technique is that it is only used for data with a one-to-one mapping whereas other methods work with data characterized by one-to-many mapping. On the other hand, the advanced learning methods are quite complicated and also have limitations. For example, GTM is used when the dimension of the subspace is quite small (one or two). Bayesian NFA has a high computational load that makes it inefficient for working with high resolution images. The LLE and ISOMAP techniques are relatively simple and perform well with examples of face and object images.[5,6,10] However,

▲IS&T Member.

Received Apr. 18, 2006; accepted for publication Mar. 17, 2008; published online May 19, 2008.
1062-3701/2008/52(3)/030504/8/$20.00.

they are restricted in relation to an image size due to both very strong computational and memory requirements.

There are a few publications in which the nonlinear dimensionality reduction technique is considered in spectral images. LLE and ISOMAP analysis of spectra and color images is presented by Kulpinski.[11] Anomaly detection in spectral images by preserving spectral uniqueness in the pixels and based on a combination of k-means clustering and LLE is presented by Kim and Finkel.[12] However, these studies do not consider applications in which a learning-based technique is utilized for high resolution spectral images. A method where the low dimensional space of a high resolution spectral image is determined has recently been introduced. The method finds the low-dimensional space by dividing the image into a set of non-overlapping tiles where ISOMAP can compute an optimal subspace in a relatively short time with feasible memory requirements. The global image subspace is then defined by merging the tile subspaces.[13] However, this technique is complicated and requires an additional alignment of the tile subspaces.

In this paper we initially use the LLE and ISOMAP techniques solely for comparison purposes and only with low-resolution images due to their poor computational scaling. There is another problem with these methods in regard to image reconstruction: there is no direct and inverse parametric mapping of data between input space and low-dimensional subspace. To provide the inverse mapping needed for the reconstruction, we use a regression technique. We call LLE and ISOMAP combined with regression modified LLE and modified ISOMAP. We then compare modified LLE and ISOMAP with regressive PCA and standard PCA using low-resolution spectral images. Finally, we analyze a set of high resolution spectral images with typical scenes to test whether the first three principal components of the regressive PCA of a spectral image reproduce color more accurately than three principal components of standard PCA. The primary goal is to reduce the dimensionality of images obtained by the spectral (multichannel) acquisition systems to three components and then accurately reproduce the images. We are mainly concerned with high resolution image analysis, which is in accord with contemporary commercially available imaging systems that work with image sizes usually measured in megapixels. To compare the different techniques we mainly use two measures for estimating accuracy: spectral color difference (RMSE) and colorimetric color difference (S-CIELAB ΔE). The former is better for reconstructing the spectra in archiving applications and the latter is superior for visual observation.

This paper is arranged as follows: the next section introduces the basic concepts of regressive PCA. We then describe modified LLE and ISOMAP and consider the possible way of measuring the intrinsic dimensionality of data. Finally, the experimental results obtained by applying these methods are given and discussed.

REGRESSIVE PRINCIPAL COMPONENT ANALYSIS

Regressive PCA represents a combination of standard PCA and regression that approximates the components with smaller eigenvalues by the first components.[7] PCA reduces the data dimensionality while an approximation by regression incorporates the nonlinearity of multidimensional data.

We assume that $\mathbf{x}$ is an n-dimensional observed vector

$$\mathbf{x} = (x_1, x_2, \ldots, x_n)^T, \tag{1}$$

where T denotes the transposition and $x_1, x_2, \ldots, x_n$ are spectral components.

For PCA the vector $\mathbf{x}$ in Eq. (1) is first centered by subtracting its mean,

$$\mathbf{x} \leftarrow \mathbf{x} - \boldsymbol{\mu}, \tag{2}$$

where the symbol $\leftarrow$ represents substitution when the value of the right-hand side is computed and substituted in $\mathbf{x}$. The covariance matrix is then defined as

$$\mathbf{C} = E(\mathbf{x}\mathbf{x}^T), \tag{3}$$

where E denotes an expectation operator. PCA involves an eigen decomposition as follows:

$$\mathbf{C} = \mathbf{U}\boldsymbol{\Lambda}\mathbf{U}^T, \tag{4}$$

where $\mathbf{U} = (\mathbf{e}_1, \ldots, \mathbf{e}_n)$, $\mathbf{e}_i = (e_{i1}, \ldots, e_{in})^T$ are the eigenvectors and $\boldsymbol{\Lambda} = \mathrm{diag}(\lambda_1, \ldots, \lambda_n)$, $\lambda_1 \geq \lambda_2 \geq \cdots \geq \lambda_n$ the eigenvalues of $\mathbf{C}$. Thus the first k principal components are given by

$$\mathbf{y}_k = \mathbf{U}_k^T \mathbf{x}. \tag{5}$$

In regression, the principal components y_j are approximated using $\mathbf{y}_q$ as follows:

$$f_j(\mathbf{y}_q, \mathbf{w}) = E(y_j | \mathbf{y}_q), \tag{6}$$

where $f_j(\,)$ is a nonlinear function, $E(|\mathbf{y}_q)$ denotes a conditional expectation at a given $\mathbf{y}_q$, q is a dimension of the underlying subspace, k is a dimension of the intermediate subspace and $j = q+1, \ldots, k$, and $\mathbf{w}$ is a parametric vector or a weight vector.

The regression of y_j in Eq. (6) is defined through network mapping. The network discovers the underlying nonlinear function $f_j(\mathbf{y}_q, \mathbf{w})$. The approximated components are then given by

$$\hat{y}_j = f_j(\mathbf{y}_q, \mathbf{w}). \tag{7}$$

The approximated components replace the principal components and are an estimate of $\hat{\mathbf{y}}_k$. Finally, since $\mathbf{U}$ is an orthogonal matrix satisfying $\mathbf{U} = \mathbf{U}^T\mathbf{U} = \mathbf{I}$, reconstruction is defined as

$$\hat{\mathbf{x}} = \mathbf{U}_k \hat{\mathbf{y}}_k + \boldsymbol{\mu}. \tag{8}$$

The method is implemented as follows:

- We compute the principal components using Eqs. (2)–(5).

- We estimate the approximated components through the first principal components using Eqs. (6) and (7).
- We reconstruct data using Eq. (8).

The drawback of the method is that it cannot be used if there is a one-to-many mapping between real and approximated components. However, the data of spectral images containing the typical scenes, i.e., several color regions, is close to linear due to the central limit theorem. Regardless of a linearization of data, we assume that there is a low-degree residual nonlinearity. This makes regressive PCA attractive for data representation because this technique providing one-to-one mapping is capable of incorporating the low-degree nonlinearity of the data. The advantage of the technique is also its computational effectiveness: a short computational time and no strong memory limitations. As a result, the application field of regressive PCA overlaps the application field of standard PCA.

To solve the regression problem in Eq. (6), the regression method based on the radial basis function (RBF) (Gaussian function) is exploited.[14] The reason is that the RBF method is relatively fast and performs well. The parameters q and k are free parameters in the experiment. The number of iterations and the number of neurons needed for the regression part of RPCA and defined experimentally are 10 and 7, respectively.

MODIFIED LLE AND ISOMAP

LLE and ISOMAP are nonlinear dimensionality reduction techniques.[5,6] ISOMAP computes geodesic distance along a subspace and then uses a multidimensional scale to reduce dimensionality. The distribution structure of the data is determined by preserving the geodesic distance between the data. LLE maps the high-dimensional data to a single global low-dimensional space by preserving the neighboring relationships. The methods have been successfully utilized for reducing the dimensionality of artificial and real data.[5,6,10]

The LLE and ISOMAP techniques have no basis functions and it is, therefore, impossible to make a parametric mapping from the high-dimensional to the low-dimensional space. Furthermore, an inverse parametric mapping is also impossible. The inverse mapping is necessary for reconstructing the image. The inverse mapping proposed in Refs. 10 and 11 is unsuitable since this approach is based on the knowledge of an original image which is not available in reconstruction. Therefore, another technique for reconstruction is developed. The proposed approach is based on an approximation through the regression of input data by the data embedded in the low-dimensional space. The approximated input components are then given by

$$\hat{x}_i = f_i(\mathbf{y}_k, \mathbf{w}), \tag{9}$$

where f_i is a mapping function, $\mathbf{y}_k$ is a vector in which the elements are embedded components, and $\mathbf{w}$ is a parametric vector.

The RBF with a Gaussian function is exploited for regression where the number of iterations and the number of neurons are 10 and 7, respectively. For the parameters used for LLE the number of neighbors is 100 and the neighborhood size for ISOMAP is 1000. The results for LLE can further be improved by increasing the number of neighbors. In this case, however, the computational time increases considerably. Therefore, the number is restricted to 100.

INTRINSIC DIMENSIONALITY

The capability of the method to determine the intrinsic dimensionality of data is an important factor. In this study this parameter is utilized as a free parameter and the dimensionality measurement is partially implemented. However, due to its importance, we present a possible way for measuring the intrinsic dimensionality.

The LLE algorithm cannot detect intrinsic dimensionality. When LLE is applied, other methods are usually used for this purpose.

The ISOMAP algorithm defines the intrinsic dimensionality, for example, for the Swiss roll data, face data sets, hand images, and handwritten digits.[6] For the data sets with an essentially nonlinear data structure, ISOMAP detects the intrinsic dimensionality better than PCA. The residual variance proposed in Ref. 6 is used to estimate the intrinsic dimensionality as follows: $1-R^2(D_m, D_y)$, where R is a correlation coefficient, D_m is the Euclidean input space distance matrix (for ISOMAP this is the graph distance matrix), and D_y is the Euclidean low-dimensional space distance matrix. We are looking for the "elbow" in the curve in order to estimate the underlying dimensionality.[6]

The residual variance will also be used for PCA and RPCA.

EXPERIMENTS

Two image sets are used as test images. Apart from *toys* and *cars*, the low-resolution images are taken from the Colorlab Toolbox of the University of Joensuu (Finland).[15] The high resolution images are taken from the Toolbox of Chiba University (Japan) (CD-ROM).[16] For all images, the S-CIELAB values are calculated from spectral images using XYZ (1931) values. The source spectral images appear as reflectance values. The illuminant D65 is used. The Intel Pentium (R) D Processor, 2.80 GHz, 0.99 GB RAM, and MATLAB are used to measure the computational time for the algorithms.

EXPERIMENTS WITH LOW RESOLUTION IMAGES

The purpose of this experiment is to compare the different learning-based techniques to better understand the properties of regressive PCA, which will be utilized in the test with high resolution images.

The spectral components of low-resolution images are evenly taken in the range 380–780 nm. The images are down sampled to the size: $64\times48\times81$ (width, height, and spectral dimension) (*fruitsandflowers*), $57\times40\times81$ (*colorchecker*), $45\times57\times81$ (*toys*), and $58\times36\times81$ (*cars*) in order to test them using LLE and ISOMAP. Figure 1 shows the low-resolution test images.

LLE and ISOMAP can work with the image sizes larger than the image sizes used in this study. However, in this case,

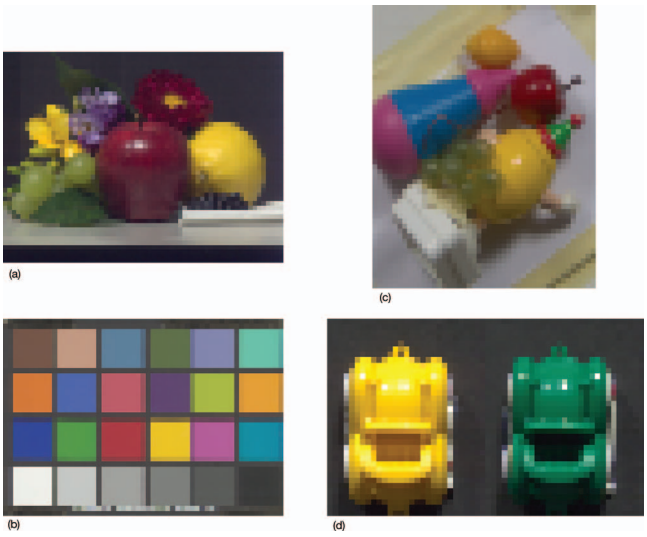

Figure 1. RGB-representation of the low-resolution images. (a) *fruitsandflowers*, (b) *colorchecker*, (c) *toys*, and (d)*cars*.

Figure 2. *fruitsandflowers*. RGB-representation of the results of reconstruction for LLE (first row), ISOMAP (second row), PCA (third row), RPCA1 (fourth row), and RPCA2 (fifth row). The first, second, third, and fourth columns correspond to the first PC, the first two PCs, the first three PCs, and the first four PCs, respectively.

computational time is increased. In addition, a larger neighborhood size means lower computation speed. Therefore, to provide both the best neighborhood size, which can be rather large, and fast computation, the test images are downsampled.

This first experiment is conducted with the low-resolution images using modified LLE (MLLE), modified ISOMAP (MISOMAP), regressive PCA (RPCA), and standard PCA (PCA). In this study, the number of PCs is used as a free parameter. This number changes from one to four and the algorithm performance related to the number of PCs is measured. To evaluate the algorithm performance, the S-CIELAB ΔE measure, the RMSE (over all pixels), and the residual variance measure are used.[17,6] The cost of the different methods is evaluated using a computational time and a compression ratio. MLLE, MISOMAP, and RPCA produce slightly different results each time we run the corresponding learning algorithm. For each measurement we run each algorithm just once.

The reconstruction results for *fruitsandflowers* are shown in Fig. 2. The results for MLLE, MISOMAP, PCA, RPCA1, and RPCA2 are shown in the first, second, third, fourth, and fifth rows, respectively. In Fig. 2, columns one to four represent image reconstruction for the first, first two, first three, and first four principal (embedded) components, respectively. RPCA1 uses $q=1$ and $k=2$, $q=2$ and $k=3$, $q=3$ and $k=4$, and $q=4$ and $k=5$ to obtain the results in the first, second, third, and fourth column in Fig. 2, respectively. RPCA2 uses $q=1$ and $k=3$, $q=2$ and $k=4$, $q=3$ and $k=5$, and $q=4$ and $k=6$ to obtain the results in the first, second, third, and fourth column in Fig. 2, respectively. The S-CIELAB ΔE and RMSE, a computational time and a compression ratio, are given in Tables I–IV, respectively. In Table III, the embedding time is the time for computing the principal (embedded) components and total time means the time for embedding and reconstruction. The residual variance of *fruitsandflowers* is shown in Fig. 3. The "elbow" in the residual variance curve indicates the point for estimating the underlying dimensionality.[6] The dimensionality of the subspace ISOMAP defined is 4. This result is in agreement with visual estimation. The cuts of the image representing the grape and the color differences (error maps) are given in

Table I. S-CIELAB ΔE (average/maximum). Numbers in cells from top to bottom are given for the first PC, the first two PCs, the first three PCs, and the first four PCs, respectively.

Method	MLLE	MISOMAP	PCA	RPCA1	RPCA2
fruits	13.39/46.44	12.93/43.88	16.89/49.15	13.80/43.46	13.51/42.72
and	6.76/32.44	6.82/36.56	12.13/43.19	7.03/33.83	6.76/35.54
flowers	4.30/17.20	3.47/17.44	4.28/17.41	3.66/14.95	3.50/14.51
	3.56/13.97	2.24/12.13	2.01/9.18	1.95/8.65	1.95/9.01
color	14.33/55.79	13.12/38.30	14.51/35.60	13.48/34.77	13.54/39.35
checker	10.21/42.83	8.89/34.78	10.41/40.47	10.20/42.92	9.80/36.04
	10.21/35.48	3.32/26.04	4.48/24.17	4.06/21.90	3.53/25.04
	9.61/36.15	2.67/25.11	2.80/13.14	2.11/11.42	2.48/11.51
toys	11.39/42.65	11.20/41.51	11.93/40.95	11.81/41.77	11.21/41.29
	5.69/40.43	6.36/31.23	7.39/48.59	6.56/34.48	6.64/34.35
	2.47/21.33	1.51/10.85	1.58/9.01	1.48/9.82	1.46/9.71
	2.08/21.70	1.59/10.95	0.82/6.12	0.79/5.88	0.79/5.91
cars	9.81/44.51	13.50/54.63	13.06/41.38	12.89/57.90	13.11/56.39
	4.24/16.64	5.15/14.83	8.68/21.83	5.40/14.63	5.64/15.43
	5.33/21.47	1.94/7.35	1.58/6.04	1.44/5.29	1.45/5.27
	4.54/19.37	1.95/8.68	1.31/5.29	1.47/5.74	1.41/6.12

Table II. RMSE. Numbers in each cell from top to bottom are given for the first PC, the first two PCs, the first three PCs, and the first four PCs, respectively.

Method	MLLE	MISOMAP	PCA	RPCA1	RPCA2
fruitsandflowers	0.0762	0.0691	0.0784	0.0709	0.0694
	0.0438	0.0315	0.0447	0.0332	0.0315
	0.0277	0.0255	0.0260	0.0243	0.0246
	0.0245	0.0198	0.0169	0.0169	0.0169
colorchecker	0.1319	0.0870	0.1025	0.0888	0.0878
	0.10	0.0536	0.0594	0.0551	0.0551
	0.0915	0.0281	0.0310	0.0301	0.0257
	0.0718	0.0260	0.0247	0.0227	0.0208
toys	0.0508	0.0494	0.0523	0.0501	0.0496
	0.0365	0.0232	0.0258	0.0234	0.0232
	0.0153	0.0125	0.0126	0.0117	0.0117
	0.0135	0.0122	0.0098	0.0097	0.0097
cars	0.0561	0.0495	0.0573	0.0512	0.0497
	0.0258	0.0198	0.0285	0.212	0.0208
	0.0351	0.0174	0.0181	0.0178	0.0170
	0.0434	0.0164	0.0135	0.0126	0.0124

Table III. Total computation time (upper number) and time for embedding (lower number) given for MLLE and MISOMAP (*fruitsandflowers*).

Method	MLLE	MISOMAP	PCA	RPCA1	RPCA2
Time, s	1944	167	0.12	0.50	0.91
	1914	144			

Table IV. A compression ratio (*fruitsandflowers*).

Method	1 PC	2 PCs	3 PCs	4 PCs
MLLE and MISOMAP	3.65	3.38	3.15	2.95
PCA	76.94	38.95	26.08	19.60
RPCA1	60.42	34.09	23.74	18.21

Fig. 3. The error maps are computed using the S-CIELAB ΔE truncated for values greater than 10. The values are then scaled from 0 to 255. Adding the fourth principal component improves the color of the grape, making it close to the original and, thus, reducing the color difference. The dimensionality found by PCA and RPCA1 is not so obvious. The dimensionality seems to be 5.

Dimensionality reduction techniques like LLE and ISOMAP have three limitations.[18] First, the manifold must be well sampled or data must be densely populated in the manifold. Second, noise can prevent correct learning. Third, for high-dimensional data, the first two problems become more severe. In our study, the sensors we used have a high signal-to-noise ratio. Spectral color data is restricted to the region having lower dimensionality. Thus, the last two problems are not considered. However, the first problem is valid. In their study, Kim and Finkel[12] concluded that the existence of several disjointed objects in the low resolution image challenges the manifold learning. In our case the test low resolution images have many color objects. In general, the S-CIELAB ΔE and RMSE results are, thus, not so good for MLLE and MISOMAP. However, the learning-based methods have relatively good results in comparison with PCA, especially for the first one, first two, and first three PCs at visual observation (Fig. 2). MISOMAP shows the average colorimetric color differences and the spectral color differences better for one, two, and three principal components than PCA. Colorimetric color differences and spectral color differences by MISOMAP for one, two, and three principal components are comparable with colorimetric color differences and spectral color differences by RPCA1 and RPCA2. The MISOMAP results are sometimes close to the results produced by RPCA2. Figure 2 illustrates the visual similarity between these two approaches. Although MLLE is not as good as other approaches, its results can be further improved at the expense of computational time. We can expect the best algorithmic performance by MLLE and MISOMAP in images containing an object described by the dichromatic

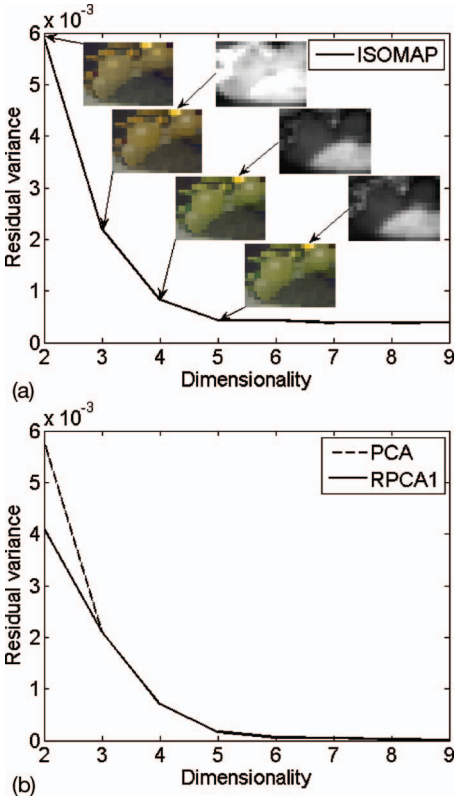

Figure 3. The residual variance computed using *fruitsandflowers*. (a) ISOMAP. (b) PCA and RPCA. The image cuts together with error maps measured from the corresponding cuts are shown in the top plot. ISOMAP reliably determines the data dimensionality while the results produced by PCA and RPCA are not so clear. For the first PC the residual variance is 0.059, 0.058, and 0.041 for ISOMAP, PCA, and RPCA, respectively.

reflection model. In this case, the data structure considered represents one nonlinear global cluster with densely distributed samples and the intrinsic dimensionality of data is one.[9] LLE and ISOMAP are also effective for images (for example, *cars*), where the number of color regions is small and the intrinsic dimensionality of data is low.

Recently, Funt et al.[19] studied nonlinear embeddings of reflectance spectra in their datasets. They concluded that the reflectance spectra lie in a nonlinear subspace with a dimensionality of 3 and ISOMAP is useful in determining the dimensionality of the data. Our experiments using the residual variance found by ISOMAP show that the nonlinear subspace dimensionality is 4 for *fruitsandflowers* (Fig. 3), 3 for *colorchecker*, 3 for *toys*, and 2 for *cars*. This also explains the fact that the learning methods are most effective for low-dimension subspaces. It is interesting to note that *colorchecker* has more colors and less dimensionality than *fruitsandflowers*. This is due to the fact that all colors in *colorchecker* are presented in equal proportions. In this sense the result for *colorchecker* is close to that for reflectance spectra. In experiments with high resolution images, this problem will be addressed one more time.

Next, we discuss measurements only for *fruitsandflowers*. Tables III and IV present computational time and compression ratio. As can be seen from these tables, the MLLE method has the longest computational time and a small compression ratio. The computational time consumed by the LLE algorithm even without mapping is long (1914 s). As displayed in Tables III and IV, the MISOMAP method also has a long computational time and a small compression ratio. The computational time of the ISOMAP algorithm excluding the inverse mapping procedure is also long (144 s). The poor value of the compression ratio for modified LLE and ISMAP is explained by the small size of the image and the need for a large number of network data structure sets equal to the number of data components. PCA has the best compression ratio, as shown in Table IV, and the best computational time.

Both RPCA1 and RPCA2 are referred to as RPCA because their results are close to each other. In most cases, RPCA demonstrates better results than LLE, ISOMAP, and PCA. RPCA is superior to PCA for the first PC and the first two PCs and gives slightly better results for the first three and the first four PCs, which can be seen in Fig. 2 and Table I. Table II shows that the spectral differences are minimal for RPCA and Table III demonstrates that the RPCA algorithm is rather fast. The compression ratio for RPCA is lower in comparison to PCA. RPCA cannot be used for computing the dimensionality of the data structure. Finally, we can conclude that RPCA performs well and is computationally efficient. Only PCA and RPCA will be used in the following study with high resolution spectral images.

EXPERIMENTS WITH HIGH RESOLUTION IMAGES

The second experiment is conducted with high resolution images using standard PCA and regressive PCA. The set of images is shown in Fig. 4 and includes p1 (*Chart*), p2 (*Oil Paint*), p3 (*Japanese Paint*), p4 (*Standard Image*), p5 (*Portrait*), p6 (*Fruit*), p7 (*Gloss Image*), and p8 (*Wool*). The size of the high resolution images acquired with a five-band camera is 764×508 (width and height) for p1–p4, p6, p7 and 508×764 for p5 and p8.

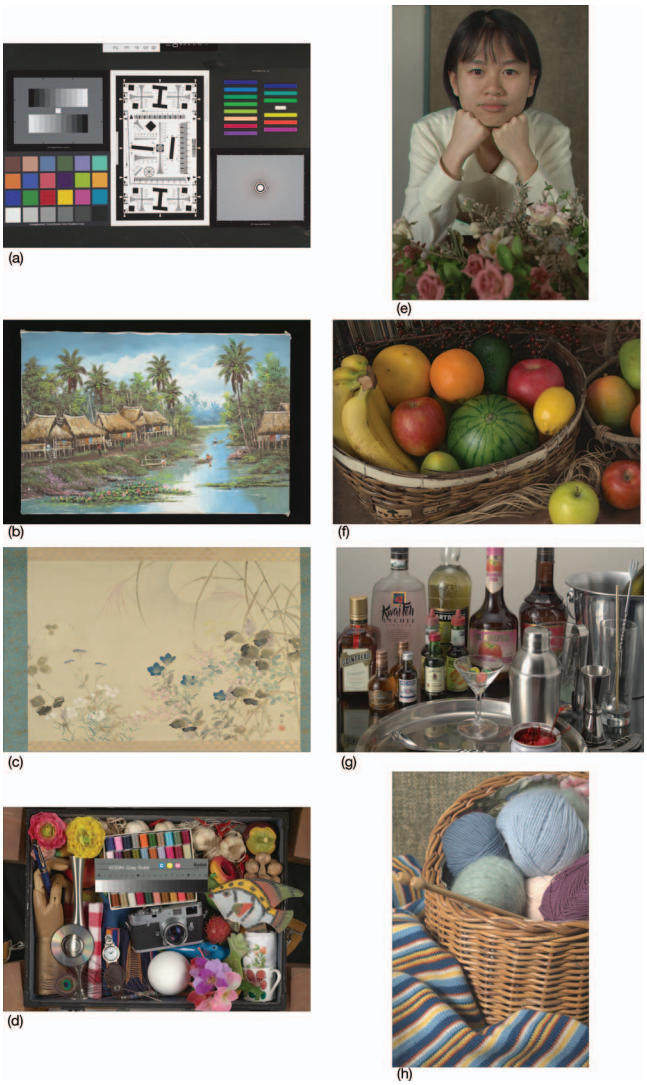

Figure 4. The set of high resolution images. (a) p1 (*Chart*), (b) p2 (*Oil Paint*), (c) p3 (*Japanese Paint*), (d) p4 (*Standard Image*), (e) p5 (*Portrait*), (f) p6 (*Fruit*), (g) p7 (*Gloss Image*), and (h) p8 (*Wool*).

The number of PCs from one to four is varied in the next experiment. We are particularly interested in whether three PCs of RPCA give (visually and quantitatively) better results than three PCs of standard PCA.

Table V shows the S-CIELAB ΔE values for PCA and RPCA. RPCA has better results for most cases. On the basis of this table and results obtained in the experiment with the low-resolution images we can conclude that the difference in color reproduction between RPCA and standard PCA is reduced by increasing the number of PCs. It is also evident that RPCA with n PCs cannot produce results better than standard PCA with $n+1$ PCs. Table VI indicates that the RMSE values obtained by using RPCA are less than the PCA values.

Table V. S-CIELAB ΔE (average/maximum) for PCA (upper number) and RPCA (lower number).

Image	PCA: 1 PC RPCA: $q=1$ $k=2$	PCA: 2 PCs RPCA: $q=2$ $k=3$	PCA: 3 PCs RPCA: $q=3$ $k=4$	PCA: 4 PCs RPCA: $q=4$ $k=5$
p1	5.69/99.56	4.30/54.50	2.73/33.46	0.44/8.33
	6.24/98.74	4.34/51.24	1.52/21.06	0.38/7.93
p2	8.34/44.79	3.18/22.34	0.84/9.19	0.70/9.30
	5.93/47.64	2.52/26.88	0.71/8.97	0.62/9.16
p3	2.63/29.94	1.48/29.98	0.66/13.18	0.16/2.42
	2.48/37.22	1.33/15.76	0.59/14.26	0.16/2.79
p4	10.99/103.85	6.38/74.34	4.30/48.21	0.53/9.86
	10.02/101.03	6.23/71.33	3.70/43.72	0.53/9.68
p5	5.07/27.00	2.99/25.60	2.72/22.05	0.73/7.90
	5.00/26.94	3.07/25.72	2.38/19.87	0.69/8.39
p6	9.88/89.94	9.04/77.87	5.50/42.77	1.35/18.08
	9.73/92.50	8.23/55.49	4.29/33.71	1.25/14.47
p7	4.41/43.97	2.55/36.36	1.11/29.42	0.74/15.78
	4.40/43.64	2.38/37.73	1.13/29.09	0.69/13.15
p8	12.46/56.86	4.46/24.56	2.39/17.39	0.22/1.49
	12.11/55.63	4.27/23.03	2.09/16.40	0.21/1.64

Table VI. RMSE. PCA (upper number) and RPCA (lower number).

Image	PCA: 1 PC RPCA: $q=1$ $k=2$	PCA: 2 PCs RPCA: $q=2$ $k=3$	PCA: 3 PCs RPCA: $q=3$ $k=4$	PCA: 4 PCs RPCA: $q=4$ $k=5$
p1	0.0285	0.0192	0.0062	0.0027
	0.0278	0.0186	0.0044	0.0023
p2	0.0273	0.0120	0.0033	0.0022
	0.0242	0.0109	0.0028	0.0020
p3	0.0201	0.0073	0.0026	0.0008
	0.0174	0.0065	0.0022	0.0008
p4	0.0391	0.0249	0.0092	0.0044
	0.0369	0.0235	0.0086	0.0043
p5	0.0180	0.0093	0.0062	0.0035
	0.0175	0.0091	0.0058	0.0034
p6	0.0364	0.0264	0.0114	0.0036
	0.0352	0.0232	0.0101	0.0035
p7	0.0182	0.0115	0.0042	0.0026
	0.0179	0.0101	0.0040	0.0022
p8	0.0453	0.0204	0.0054	0.0023
	0.0445	0.0186	0.0049	0.0022

We then compute the error maps of the test images using PCA with the first three PCs and RPCA with parameters $q=3$ and $k=4$. Figures 5 and 6 show the error maps for PCA and RPCA, respectively. As in the first experiments, the error maps of the test images are computed using the S-CIELAB ΔE. The error values greater than10 are truncated. The error values are then scaled from 0 to 255. The error maps computed from images p1, p3, p5, p6, and p8 are better for RPCA than for PCA. It is difficult to compare the error maps of p2, p4, and p8.

In summarizing the results from both experiments one observation must be made. The images *fruitsandflowers*, p6 and p8, are difficult to represent using three principal components by the tested methods. These images contain several color regions, which are very different. In these images only gray, yellow, brown, red, cyan, and blue are reproduced close to the original image. Green and magenta are poorly reconstructed. The analysis made for *fruitsandflowers* shows that the first eigenvector is relatively smooth and relates to a gray color. The second and third eigenvectors have only one dominant transition between low spectral values and high spectral values. This is the case of yellow, brown, red, blue, and cyan. The fourth eigenvector has two dominant transitions and is responsible for reconstructing green and magenta. Although RPCA incorporates information from the weak components, RPCA is not efficient enough for learning green and magenta colors. In our future study we will address this problem.

The average computation time measured for the image set for PCA (3 PCs) is approximately 0.78 s, and for RPCA ($q=3$ and $k=4$) 52.25 s. The compression ratio for high resolution images is 1.66 for PCA (3 PCs) and for RPCA ($q=3$ and $k=4$). The compression ratio values for both methods are approximately equal because the network data structure size required by RPCA is small in comparison to the size of the principal components of a high resolution image. PCA is faster than RPCA.

The experiments confirm the improvements in the reconstructed images obtained through the use of RPCA. Thus, it is very useful in spectral image processing where the number of components is reduced and image processing algorithms are applied to them. The utilization of this method saves computational time and memory. The merit of the technique is that the reconstructed image includes information not only from the retained principal components but also partial information from weak (approximated) components. Hence, RPCA reproduces colors (up to four principal components) more accurately than PCA, requires approximately the same memory in applications with high resolution images, and is relatively fast.

CONCLUSIONS

In this paper, the comparative study of several dimensionality reduction approaches for low-resolution and high reso-

Figure 5. Error maps of the test images (PCA).

Figure 6. Error maps of the test images (RPCA).

lution spectral images was presented. The study shows that the existence of several color regions makes learning difficult for LLE and ISOMAP. However, ISOMAP produces more desirable results (both ΔE and RMSE) for one, two, and three principal components than PCA. In addition, ISOMAP correctly finds the dimensionality of a nonlinear subspace. The dimensionality found by ISOMAP is in agreement with visual estimation. LLE and ISOMAP are a computational burden. In most cases, RPCA has the best spectral and color differences than other approaches. RPCA reproduces colors (up to four principal components) more accurately than PCA. This is especially important in applications with high resolution images since RPCA is computationally efficient. RPCA cannot be used to determine the dimensionality of data. In addition, RPCA with n components does not produce a result better than PCA with $n+1$ component. In our future study we will address this problem.

ACKNOWLEDGMENTS

The authors thank the Academy of Finland for the funding granted to this study.

REFERENCES

[1] Y. Miyake, "Evaluation of image quality based on human visual characteristics", *Proc. First International Workshop on Image Media Quality and its Applications*, (Nagoya, Japan, 2005) pp. 10–14.
[2] L. W. MacDonald, "Colour engineering in digital imaging", *Proc. First CGIV* (IS&T, Springfield, VA, 2000) pp. 358–363.
[3] C. M. Bishop, M. Swensen, and C. K. I. Williams, "GTM: The generative topographic mapping", Neural Comput. **10**, 215–234 (1998).
[4] H. Lappalainen and A. Honkela, "Bayesian nonlinear independent component analysis by multi-layer perceptrons," in *Advances in Independent Component Analysis*, edited by M. Girolami (Springer, Berlin, 2000), pp. 93–121.
[5] S. T. Roweis and L. K. Saul, "Nonlinear dimensionality reduction by locally linear embedding", Science **290**, 2323–3236 (2000).
[6] J. B. Tenenbaum, V. de Silva, and J. C. Langford, "A global geometric framework for nonlinear dimensionality reduction," Science **290**,

2319–2323 (2000).
[7] V. Bochko and J. Parkkinen, "Principal component analysis using approximated principal components", *Research Report* 90, (Department of Information Technology, Lappeenranta University of Technology, Finland, 2004), pp. 1–7.
[8] V. Bochko, N. Tsumura, and Y. Miyake, "Spectral color imaging system for estimating spectral reflectance of paint", J. Imaging Sci. Technol. **51**(5), 70–78 (2007).
[9] V. Bochko and J. Parkkinen, "A spectral color analysis and colorization technique", IEEE Comput. Graphics Appl. **26**(5), 74–82 (2006).
[10] Y. C. Zhang, J. Wang, N. Zhao, and D. Zhang, "Reconstruction and analysis of multi-pose face images based on nonlinear dimensionality reduction", Pattern Recogn. **37**, 325–336 (2004).
[11] D. Kulpinski, "LLE and ISOMAP analysis of spectra and color images", Master's Thesis, School of Computer Science, Simon Fraser University (2002).
[12] D. H. Kim and L. H. Finkel, "Hyperspectral image processing using locally linear embedding", *Proc. First International IEEE EMBS Conference on Neural Engineering* (IEEE, Piscataway, NJ, 2003), pp. 316–319.
[13] C. M. Bachmann, T. L. Ainsworth, and R. A. Fusina, Exploiting manifold geometry in hyperspectral imagery", IEEE Trans. Geosci. Remote Sens., **GE-43**(3), 441–454 (2005).
[14] I. T. Nabney, *Netlab Algorithms for Pattern Recognition* (Springer, Berlin, 2002).
[15] Spectral Database, University of Joensuu Color Group, http://spectral.joensuu.fi/
[16] *Introduction to Multispectral Imaging*, edited by Y. Miyake (University of Tokyo Press, Tokyo, 2006) (in Japanese).
[17] X. Zhang and B. A. Wandell, "A spatial extension of CIELAB for digital color image reproduction", Proc. SID Symp. Tech. Digest **27**, 731–734 (1996).
[18] M.-C. Yeh, I.-H. Lee, G. Wu, Y. Wu, and E. Y. Chang, "Manifold learning: A promised land or work in progress?", in *Proc. IEEE International Conference on Multimedia and Expo* (IEEE, Piscataway, NJ, 2005), pp. 1154–1157.
[19] B. Funt, D. Kulpinski, and V. Cardei, "Non-linear embeddings and the underlying dimensionality of reflectance spectra and chromaticity histograms", *Proc. IS&T/SID 9th Color Imaging Conf.* (IS&T, Springfield, VA, 2001), pp. 126–129.